

Floquet approach to bichromatically driven cavity optomechanical systems

Daniel Malz and Andreas Nunnenkamp

Cavendish Laboratory, University of Cambridge, Cambridge CB3 0HE, United Kingdom

(Dated: November 8, 2018)

We develop a Floquet approach to solve time-periodic quantum Langevin equations in steady state. We show that two-time correlation functions of system operators can be expanded in a Fourier series and that a generalized Wiener-Khinchin theorem relates the Fourier transform of their zeroth Fourier component to the measured spectrum. We apply our framework to bichromatically driven cavity optomechanical systems, a setting in which mechanical oscillators have recently been prepared in quantum-squeezed states. Our method provides an intuitive way to calculate the power spectral densities for time-periodic quantum Langevin equations in arbitrary rotating frames.

I. INTRODUCTION

In a recent breakthrough, quantum squeezing of a mechanical oscillator has been demonstrated experimentally [1–3]. The method has been analyzed first in Ref. [4], but its full potential was realized in Ref. [5]. It involves a standard optomechanical setup, comprising an optical cavity coupled to a mechanical oscillator, where the cavity mode is subject to unequally strong driving on both upper and lower mechanical sidebands. This results in a Hamiltonian and consequently quantum Langevin equations that are explicitly periodic in time. Solving those is more difficult than stationary ones, since in general solutions contain all multiples of the fundamental frequency.

In this article, we develop a simple, yet powerful approach to find the steady state of the bichromatically driven optomechanical system based on Floquet theory. In effect, all system operators are split up into Fourier components, which individually obey stationary quantum Langevin equations. As a result, any two-time correlation function of system operators $C(\tau, t) = \langle \hat{A}(t + \tau) \hat{B}(t) \rangle$ is periodic in time t and can be expressed in Fourier components, a property that carries over to its Fourier transform $S(\omega, t)$. Although a typical measurement only returns its time average, i.e., the zeroth Fourier component of $S(\omega, t)$, the rotating components may carry information, as is the case for dissipative squeezing [1–3, 5].

Within our framework, we derive analytical expressions for the mechanical and optical spectrum within the rotating-wave approximation (RWA) for general detunings. With the expressions for the Fourier components of system operators we provide, it is straightforward to construct the spectrum in an arbitrary rotating frame. This enables us to understand dynamical effects that occur when the drives are not exactly on the sidebands, for example, how squeezing generation can fail or fail to be detected. We show that there is a special frame in which rotating components become part of the stationary spectrum and can be directly observed. The method also elucidates how information about the system can be extracted through a second, bichromatically driven “readout” mode, an approach used in the experiments reported in Ref. [3]. Our framework will be useful for other explicitly time-periodic quantum Langevin equations and provides an intuitive way to understand power spectral densities in arbitrary rotating frames.

The remainder of this article is organized as follows. In

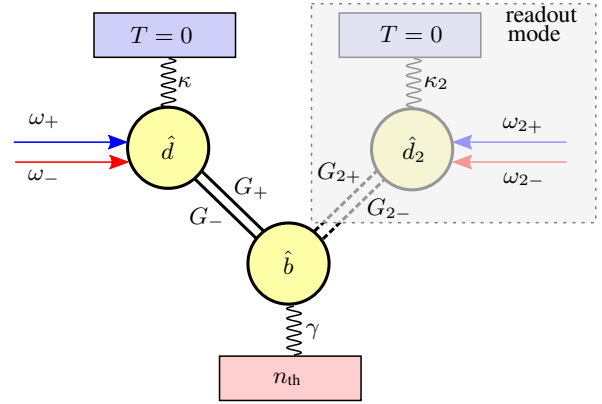


FIG. 1. **Schematic of linearized quantum Langevin equations** (4a) and (4b). The yellow circles depict harmonic oscillators, namely the mechanical mode with annihilation operator \hat{b} and two optical modes \hat{d} and \hat{d}_2 , respectively. The optical modes are coupled to the mechanical mode via radiation pressure (straight lines). Both optical modes are driven bichromatically, which leads to enhanced optomechanical coupling strengths G_{\pm} and $G_{2\pm}$. The optical modes are also coupled to independent zero-temperature baths (blue) with rate κ and κ_2 , respectively. We will not consider the readout mode until Sec. IV. The mechanical mode is coupled to its own bath at a finite temperature (red) with a mean occupation n_{th} and at a rate γ .

Sec. II we describe the model and our framework, how to obtain the solution, and familiarize ourselves with the properties of spectrum Fourier components. Section III exemplifies the technique through detailed analysis of dissipative squeezing. This is followed by Sec. IV, which is concerned with the readout of the state of the mechanical oscillator through a second cavity mode. Finally, we conclude in Sec. V.

We note that Floquet theory has been developed on the level of the covariance matrix for an cavity optomechanical system with modulated coupling strength [4] as well as on the level of quantum master equations for numerical simulations of, for example, cavity quantum electrodynamics in Ref. [6].

$$\begin{pmatrix} \ddots & & & & & \\ & \vdots & & & & \\ \cdots & i(\omega + \delta) + A^{(0)} & A^{(-1)} & & & \\ \cdots & A^{(1)} & i\omega + A^{(0)} & A^{(-1)} & & \\ \cdots & A^{(2)} & A^{(1)} & i(\omega - \delta) + A^{(0)} & \cdots & \\ & \vdots & & & \ddots & \end{pmatrix} \begin{pmatrix} \vdots \\ \mathbf{x}^{(-1)} \\ \mathbf{x}^{(0)} \\ \mathbf{x}^{(1)} \\ \vdots \end{pmatrix} = \begin{pmatrix} \vdots \\ 0 \\ -\mathbf{F}_{\text{in}} \\ 0 \\ \vdots \end{pmatrix}. \quad (10)$$

In our case, only $A^{(0,\pm 1)}$ are non-zero. In the general case, one has to truncate the infinite matrix (10) to find an approximate solution. In RWA the infinite set of equations decouples in sets of four, making the problem tractable analytically, see Sec. III. Equation (10) provides a visual tool for analyzing how the 4-by-4 blocks in each entry are coupled to each other, which can be exploited to design new driving schemes. For example, a block such as $A^{(n)}$ can be “activated” by either having an anharmonic drive with a nonzero n th Fourier component, or by adding a laser with frequency $\omega_- + n\delta$. For details on how these matrices look like in general, see Appendix A.

The advantage of splitting system operators up into Fourier components is that these are governed by stationary quantum Langevin equations and thus have time-independent expectation values and time-translation invariant correlation functions. Therefore, any combination of Fourier components will have a well-defined spectrum from which the measured spectra can be obtained in any rotating frame.

B. Spectrum Fourier components

One might ask which implications the time-periodicity of the quantum Langevin Eqs. (4a) and (4b) has on the properties of the measured spectra. As has been alluded to above, the Fourier transform of the autocorrelator consists of Fourier components and thus is not time-translation invariant. In this section we introduce these Fourier components and mention some of their properties. Finally, in a slight generalization of the Wiener-Khinchin (WK) theorem, we show that the time-averaged power spectrum is the Fourier transform of the zeroth Fourier component of the autocorrelator.

First, let us define

$$S_{A^\dagger A}(\omega, t) \equiv \int_{-\infty}^{\infty} d\tau e^{i\omega\tau} C_{AA}(\tau, t), \quad (11)$$

where $C_{AA}(\tau, t) = \langle A^\dagger(t + \tau)A(t) \rangle$ is an autocorrelator. We expect the steady state to be periodic, with period $2\pi/\delta$ [10]. Therefore, $S_{A^\dagger A}(\omega, t)$ can be expressed as a Fourier series

$$S_{A^\dagger A}(\omega, t) = \sum_{n=-\infty}^{\infty} e^{in\delta t} S_{A^\dagger A}^{(n)}(\omega) \quad (12)$$

with Fourier components

$$S_{A^\dagger A}^{(m)}(\omega) = \sum_{n=-\infty}^{\infty} \int \frac{d\omega'}{2\pi} \langle A^{(n)\dagger}(\omega + n\delta) A^{(m-n)}(\omega') \rangle. \quad (13)$$

By construction, the spectrum Fourier components encode all information about the autocorrelator $C_{AA}(\tau, t)$. We will often refer to $S_{A^\dagger A}(\omega, t)$ as “spectrum” although technically it is not a power spectrum in general. As we will show in Appendix B, in any given frame, the stationary part $S_{A^\dagger A}^{(0)}$ is the physical power spectrum whereas other Fourier components $S_{A^\dagger A}^{(m \neq 0)}$ average out for long measurement times. This generalization of the WK theorem is consistent with the stationary case, where all Fourier components apart from the zeroth one vanish. In one special rotating frame the rotating components become stationary and can be directly measured, see Sec. II C.

Moreover, we can show that (proof in Appendix C)

$$\left[S_{A^\dagger B}^{(n)}(\omega) \right]^\dagger = S_{B^\dagger A}^{(-n)}(\omega + n\delta). \quad (14)$$

The stationary spectrum $S_{A^\dagger A}^{(0)}(\omega)$ is thus real, but the other spectrum Fourier components are complex in general.

Finally, we would like to mention that one can regard $S_{A^\dagger A}(\omega, t)$ as a distribution of energy in time and frequency. Its marginal distributions are the stationary part

$$S_{A^\dagger A}^{(0)}(\omega) = \lim_{T \rightarrow \infty} \left[\frac{1}{T} \int_0^T dt S_{A^\dagger A}(\omega, t) \right], \quad (15)$$

and the variance as a function of time

$$\langle |A(t)|^2 \rangle = \int_{-\infty}^{\infty} \frac{d\omega}{2\pi} S_{A^\dagger A}(\omega, t), \quad (16)$$

both of which are guaranteed to be real and positive.

C. The spectrum in a rotating frame

Although the rotating components of the spectrum drop out of the lab frame spectrum, they can be observed in a special rotating frame. In this section we show how rotating frames and spectra are expressed in our framework.

Let us start by defining a quadrature rotating at frequency ν and with an additional phase ϑ [12]

$$\begin{aligned} X_\nu^\vartheta(t) &\equiv b(t)e^{i\nu t + i\vartheta} + b^\dagger(t)e^{-i\nu t - i\vartheta} \\ &= \sum_n e^{in\delta t} \left(b^{(n)}(t)e^{i\nu t + i\vartheta} + b^{(n)\dagger}(t)e^{-i\nu t - i\vartheta} \right). \end{aligned} \quad (17)$$

The autocorrelator of the rotating quadrature contains components rotating at $n\delta$ and $n\delta \pm 2\nu$ in general

$$S_{X_\nu^\vartheta X_\nu^\vartheta}(\omega, t) = \sum_{n,m} e^{i(n+m)\delta t} \times \left[f_{bb}(n, m, \omega + n\delta + \nu) e^{2i(\nu t + \vartheta)} + f_{b^\dagger b^\dagger}(n, m, \omega + n\delta - \nu) e^{-2i(\nu t + \vartheta)} + f_{bb^\dagger}(n, m, \omega + n\delta + \nu) + f_{b^\dagger b}(n, m, \omega + n\delta - \nu) \right], \quad (18)$$

where we have introduced the shorthand

$$f_{A^\dagger B}(n, m, \omega) \equiv \int d\tau \exp(i\omega\tau) \left\langle A^{(n)\dagger}(t + \tau) B^{(m)}(t) \right\rangle. \quad (19)$$

Note that the RHS of Eq. (19) does *not* depend on the time t . The Fourier components $A^{(n)}$, $B^{(m)}$ are given by Langevin equations without explicit time-dependence and thus their correlator is time-translation invariant. Note that the sum $n + m$ tells us which lab frame spectrum component $f(n, m, \omega)$ belongs to, as per Eq. (13).

Equation (18) makes it clear that the case $\nu = \delta/2$ is special, since in that case the terms $f_{bb}(n, -n - 1, \omega + n\delta + \nu)$ and $f_{b^\dagger b^\dagger}(n, -n + 1, \omega + n\delta - \nu)$ are part of the stationary spectrum. We obtain

$$S_{X_{\delta/2}^\vartheta X_{\delta/2}^\vartheta}^{(0)}(\omega) = S_{bb^\dagger}^{(0)}(\omega + \delta/2) + S_{b^\dagger b}^{(0)}(\omega - \delta/2) + \cos(2\vartheta) \left[S_{bb}^{(-1)}(\omega + \delta/2) + S_{b^\dagger b^\dagger}^{(1)}(\omega - \delta/2) \right]. \quad (20)$$

It is real and positive. In particular, condition (14) ensures that $S_{bb}^{(-1)}(\omega + \delta/2) = [S_{b^\dagger b^\dagger}^{(1)}(\omega - \delta/2)]^*$.

The utility of these concepts will become clear in Sec. III B where we contrast spectra for dissipative squeezing in the lab frame with those in the special rotating frame, see Fig. 2.

III. DISSIPATIVE SQUEEZING IN THE ROTATING-WAVE APPROXIMATION

In this section we derive analytic expressions for the system operator Fourier components, which enables a detailed study of dissipative squeezing and simultaneously serves to illustrate the advantages of our new framework.

To obtain an analytical solution, we will neglect counterrotating terms in Eqs. (4a) and (4b), which results in

$$\begin{aligned} \dot{d} &= \left(i\Delta - \frac{\kappa}{2} \right) d + \sqrt{\kappa} d_{\text{in}} + i(G_+ e^{-i\delta t} b^\dagger + G_- b), \\ \dot{b} &= \left(-i\Omega - \frac{\gamma}{2} \right) b + \sqrt{\gamma} b_{\text{in}} + i(G_- d + G_+ e^{-i\delta t} d^\dagger). \end{aligned} \quad (21)$$

This is the rotating-wave approximation (RWA). Note that by defining $\tilde{d} = e^{i\delta t/2} d$ and $\tilde{b} = e^{i\delta t/2} b$ it is possible to write Eqs. (21) in a frame where they become stationary.

Within RWA ($\lambda = 0$) the infinite set of equations (7) decouples into sets of four. Equivalently, we can make Eq. (10) block-diagonal through a rearrangement of rows. The blocks disconnected from input operators will decay and vanish in the steady state. Thus, only two blocks (mutually hermitian conjugates) will contribute. The problem reduces to solving

$$\begin{pmatrix} \chi_c^{-1}(\omega) & -iG_- & 0 & -iG_+ \\ -iG_- & \chi_m^{-1}(\omega) & -iG_+ & 0 \\ 0 & iG_+ & \chi_c^{-1*}(-\omega + \delta) & iG_- \\ iG_+ & 0 & iG_- & \chi_m^{-1*}(-\omega + \delta) \end{pmatrix} \times \begin{pmatrix} d^{(0)}(\omega) \\ b^{(0)}(\omega) \\ d^{(1)\dagger}(\omega) \\ b^{(1)\dagger}(\omega) \end{pmatrix} = \begin{pmatrix} \sqrt{\kappa} d_{\text{in}}(\omega) \\ \sqrt{\gamma} b_{\text{in}}(\omega) \\ 0 \\ 0 \end{pmatrix}, \quad (22)$$

with the cavity and mechanical response functions $\chi_c^{-1}(\omega) = \kappa/2 - i(\omega + \Delta)$ and $\chi_m^{-1}(\omega) = \gamma/2 - i(\omega - \Omega)$, respectively.

Inverting the matrix on the left-hand side, we can write the system operators in terms of input operators

$$\begin{pmatrix} b^{(0)}(\omega) \\ b^{(1)\dagger}(\omega) \end{pmatrix} = \begin{pmatrix} a(\omega) & c(\omega) \\ f(\omega) & g(\omega) \end{pmatrix} \begin{pmatrix} b_{\text{in}}(\omega) \\ d_{\text{in}}(\omega) \end{pmatrix}. \quad (23)$$

Analytic expressions for the auxiliary functions can be found in Appendix D. Much of the physics can be understood by separating weak-coupling and strong-coupling effects, which we will discuss in turns below.

A. Weak-coupling approximation

We can gain more insight when the coupling G_\pm is small, such that second-order perturbation theory captures the main effects.

If $\Delta = -\Omega$ and writing $\delta = 2\Omega + \varepsilon$, we obtain to second order in G_\pm (see Appendix E)

$$\dot{b}^{(0)} = \left(-i\tilde{\Omega} - \frac{\tilde{\gamma}}{2} \right) b^{(0)} + \frac{2iG_-}{\sqrt{\kappa}} d_{\text{in}} + \sqrt{\gamma} b_{\text{in}}, \quad (24a)$$

$$\dot{b}^{(1)\dagger} = \left(i\tilde{\Omega} - i\delta - \frac{\tilde{\gamma}}{2} \right) b^{(1)\dagger} - \frac{2iG_+}{\sqrt{\kappa}} d_{\text{in}}, \quad (24b)$$

where

$$\tilde{\gamma} = \gamma + \frac{4}{\kappa} \left(G_-^2 - \frac{G_+^2}{1 + 4\varepsilon^2/\kappa^2} \right), \quad (25a)$$

$$\tilde{\Omega} = \Omega + \frac{G_+^2 \varepsilon}{(\kappa/2)^2 + \varepsilon^2}. \quad (25b)$$

These equations provide several insights. First, in addition to the intrinsic mechanical damping, $b^{(0)}$ is subject to ‘‘optical damping’’ [7]. At $\varepsilon = 0$, this occurs with a rate $4\mathcal{G}^2/\kappa$, where $\mathcal{G}^2 \equiv G_-^2 - G_+^2$. Since we are treating the problem in a frame where the red-detuned drive is stationary, it couples to the zeroth Fourier component with strength G_- . Crucially, the

optical input noise d_{in} has opposite signs in the two equations. The implications of that sign become clear if we consider the rotating quadrature (17)

$$X_{\nu}^0(t) = e^{i\nu t} \left[b^{(0)} + e^{-i\delta t} b^{(-1)} \right] + e^{-i\nu t} \left[b^{(0)\dagger} + e^{i\delta t} b^{(1)\dagger} \right]. \quad (26)$$

If $\delta = 2\nu$, $b^{(0)}$ and $b^{(1)\dagger}$ have the same phase factor

$$X_{\delta/2}^0(t) = e^{i\delta t/2} \left[b^{(0)} + b^{(1)\dagger} \right] + \text{h.c.}, \quad (27)$$

and Eq. (24a) gives

$$\begin{aligned} \dot{X}_{\delta/2}^0 &= -\frac{\tilde{\gamma}}{2} X_{\delta/2}^0 + \left(\frac{\delta}{2} - \tilde{\Omega} \right) X_{\delta/2}^{\pi/2} \\ &+ \left\{ e^{i\delta t/2} \left[\frac{2i}{\sqrt{\kappa}} (G_- - G_+) d_{\text{in}} + \sqrt{\gamma} b_{\text{in}} \right] + \text{h.c.} \right\}. \end{aligned} \quad (28)$$

First, as is the case for all quadratures, the effective mechanical damping has an optical contribution. Second, we see that in this particular rotating quadrature the optical noise is reduced, which is also a feature of the exact equations of motion (see minus sign on RHS of Eq. (D2) in Appendix D), and $X_{\delta/2}^0 = X_-$ is the squeezed quadrature. If $b^{(0)}$ and $b^{(1)\dagger}$ do not have the same phase factor (for $\nu \neq \delta/2$), then as time t evolves, their relative phase changes, such that sometimes the noises add and at other times they subtract, i.e., the quadrature we consider rotates relative to the squeezed and antisqueezed quadratures. Third, note that the noises only subtract because both lasers are driving the same mode and thus are subject to the same vacuum fluctuations. If in addition $G_- = G_+$, this setup performs a quantum nondemolition (QND) measurement of the rotating mechanical quadrature [13]. In (26) we could set $\vartheta = \pi/2$, which would introduce a relative minus sign between the two square brackets, such that the noises add, to give the antisqueezed quadrature X_+ . Fourth, we note that the second term in (28) contains the conjugate quadrature. It is only non-zero if $\delta \neq 2\Omega$. Essentially, the mechanical quadratures naturally rotate at the mechanical frequency Ω , so the faster we rotate relative to Ω the quicker we will catch up with the quadrature $\pi/2$ ahead. The resulting continuous mixing will play an important role in squeezing loss and heating, cf. Sections III D and III E.

We Fourier transform Eq. (24a) to obtain an approximation to Eq. (23)

$$\begin{aligned} a(\omega) &\approx \sqrt{\gamma} \tilde{\chi}_m(\omega), \\ c(\omega) &\approx 2iG_- \tilde{\chi}_m(\omega) / \sqrt{\kappa}, \\ f(\omega) &\approx 0, \\ g(\omega) &\approx -2iG_+ \tilde{\chi}_m^*(-\omega + \delta) / \sqrt{\kappa}, \end{aligned} \quad (29)$$

where we have defined $\tilde{\chi}_m^{-1}(\omega) = \tilde{\gamma}/2 - i(\omega - \tilde{\Omega})$ and again have neglected terms $\mathcal{O}(G_{\pm}^3)$. For details see Appendix E, where we also write down an effective master equation that treats the cavity as an extra bath.

Using Eqs. (13) and (29) we write down the components

that make up the mechanical spectrum for general detuning δ

$$S_{b^\dagger b}^{(0)}(\omega) = |\tilde{\chi}_m(-\omega)|^2 \left(\gamma n_{\text{th}} + \frac{4G_+^2}{\kappa} \right), \quad (30a)$$

$$S_{bb^\dagger}^{(0)}(\omega) = |\tilde{\chi}_m(\omega)|^2 \left(\gamma(n_{\text{th}} + 1) + \frac{4G_-^2}{\kappa} \right), \quad (30b)$$

$$S_{bb}^{(-1)}(\omega) = -\frac{4G_- G_+}{\kappa} \tilde{\chi}_m(\omega) \tilde{\chi}_m(-\omega + \delta), \quad (30c)$$

$$S_{b^\dagger b^\dagger}^{(1)}(\omega) = -\frac{4G_- G_+}{\kappa} \tilde{\chi}_m^*(\omega + \delta) \tilde{\chi}_m^*(-\omega). \quad (30d)$$

Integrating over the frequency ω , we arrive at

$$\int_{-\infty}^{\infty} \frac{d\omega}{2\pi} S_{b^\dagger b}^{(0)}(\omega) = \frac{\gamma n_{\text{th}} + 4G_+^2/\kappa}{\tilde{\gamma}}, \quad (31a)$$

$$\int_{-\infty}^{\infty} \frac{d\omega}{2\pi} S_{bb^\dagger}^{(0)}(\omega) = \frac{\gamma(n_{\text{th}} + 1) + 4G_-^2/\kappa}{\tilde{\gamma}}, \quad (31b)$$

$$\int_{-\infty}^{\infty} \frac{d\omega}{2\pi} S_{bb}^{(-1)}(\omega) = -\frac{4G_- G_+/\kappa}{\tilde{\gamma} - i\varepsilon}, \quad (31c)$$

$$\int_{-\infty}^{\infty} \frac{d\omega}{2\pi} S_{b^\dagger b^\dagger}^{(1)}(\omega) = -\frac{4G_- G_+/\kappa}{\tilde{\gamma} + i\varepsilon}, \quad (31d)$$

and we obtain the variance in the squeezed and antisqueezed quadratures (which are rotating at the frequency $\delta/2$)

$$\begin{aligned} \langle X_{\pm}^2 \rangle &= \frac{\gamma}{\tilde{\gamma}} (2n_{\text{th}} + 1) + \frac{4}{\kappa\tilde{\gamma}} (G_+^2 + G_-^2) \\ &\pm \frac{8G_- G_+}{\kappa\tilde{\gamma}} \left(\frac{1}{1 + \varepsilon^2/\tilde{\gamma}^2} \right), \end{aligned} \quad (32)$$

where we have defined the detuning of the higher-frequency laser from the upper mechanical sideband as $\varepsilon \equiv \delta - 2\Omega$. Term-by-term, the variance contains a reduced (if $G^2 > 0$) occupancy due to the extra optical damping, a positive term due to the noise added by the drives, and a term that can be negative due to the aforementioned noise canceling effect of the two drives in one of the quadratures, see Eqs. (24a) and (24b). In the antisqueezed quadrature, the noises add. The optically enhanced damping rate $\tilde{\gamma}$ reduces to the one for sideband cooling for $\varepsilon \gtrsim \kappa$. In that limit the last term on the RHS of Eq. (32) vanishes and the two quadratures have equal variances. Equation (32) is then very close to the expected result, apart from the extra noise term $4G_+^2/\kappa\tilde{\gamma}$, which at this level of approximation does not depend of the detuning ε .

B. Variance in the squeezed and antisqueezed quadratures

In Sec. III A we found that the quadrature in which the optical noises cancel most is the one rotating at half the laser frequency difference $\delta/2$. With the analytical solution at hand, we can go a more direct way and ask which phase ϑ will have the smallest (or largest) quadrature variance. In agreement to what we found above, ϑ will have to depend on time with angular velocity $\delta/2$.

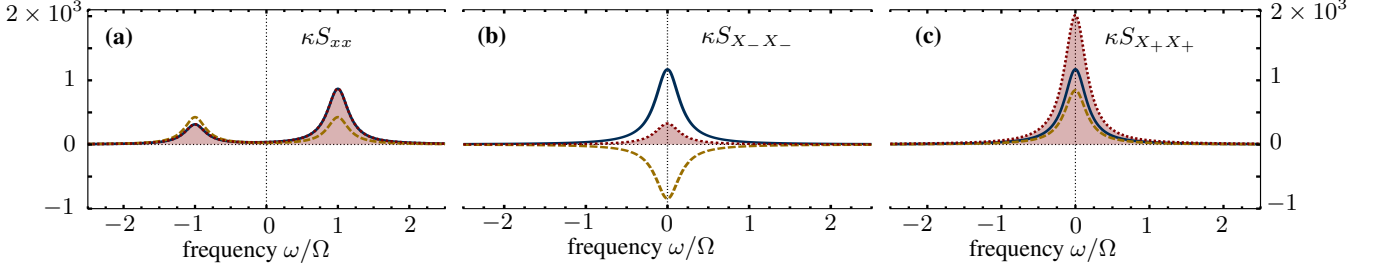


FIG. 2. **Mechanical spectrum in the lab frame and the special rotating frame.** (a) **Lab frame.** The stationary part $S_{xx}^{(0)}$ (40) is plotted in blue (solid) and has two peaks that stem from $S_{b^\dagger b}^{(0)}$ (left) and $S_{bb^\dagger}^{(0)}$ (right peak). $S_{xx}^{(0)}$ coincides with the measured spectrum for the position quadrature $x = b + b^\dagger$ (red, filled). The yellow (dashed) curve is the absolute value of the sum of the rotating components $S_{b^\dagger b^\dagger}^{(1)}$ (left peak) and $S_{bb}^{(-1)}$ (right peak), and does not contribute to the lab frame spectrum. (b), (c) **Special rotating frame.** The previously rotating spectrum components (still yellow and dashed) become stationary and thus part of the measured spectrum for the quadrature $X_{\delta/2}^\vartheta$ (red, dotted and filled), see Eq. (20). Their phase relation (encoded in ϑ) determines whether they add to the stationary part (still blue and solid) to give the antisqueezed quadrature X_+ in (c), at $\vartheta = \pi/2$, or subtract from it to yield the squeezed quadrature X_- in (b), at $\vartheta = 0$. Parameters are $\gamma/\kappa = 10^{-4}$, $n_{\text{th}} = 10$, $C = 10^2$, $\Delta = -\Omega$, $\delta = 2\Omega$. In RWA, the only effect of $\Omega/\kappa = .02$ is to determine the position of the peaks.

Let us consider a lab frame quadrature $X_{\nu=0}^\vartheta$, with variance

$$\langle (X_0^\vartheta)^2 \rangle = 1 + 2 \sum_n e^{in\delta t} \Xi_{bb}^{(n)} + 2\text{Re} \left[e^{2i\vartheta} \sum_n e^{in\delta t} \Xi_{b^\dagger b}^{(n)} \right], \quad (33)$$

where

$$\Xi_{AB}^{(n)} \equiv \int S_{A^\dagger B}^{(n)}(\omega) \frac{d\omega}{2\pi}. \quad (34)$$

Note that by Eq. (14) the second term on the RHS of Eq. (33) is always real. The variance is minimal for

$$\vartheta = \frac{\pi}{2} - \frac{1}{2} \arg \left[\sum_n e^{in\delta t} \Xi_{b^\dagger b}^{(n)} \right]. \quad (35)$$

In RWA, the only non-zero $\Xi_{b^\dagger b}^{(n)}$ is the one with $n = -1$, which turns out to be real and negative. This results in $\vartheta(t) = \delta t/2$, the squeezed quadrature is rotating. So, even though we started off not knowing that we would have to consider a rotating quadrature, the result emerged naturally.

We can calculate the maximum and minimum variance

$$\langle X_\pm^2 \rangle = 1 + 2 \sum_n e^{in\delta t} \Xi_{bb}^{(n)} \pm 2 \left| \sum_n e^{in\delta t} \Xi_{b^\dagger b}^{(n)} \right|. \quad (36)$$

For the position quadrature $x = X_0^{\vartheta=0}$ and in RWA, we obtain

$$\langle x(t)^2 \rangle = 1 + 2\Xi_{bb}^{(0)} + 2|\Xi_{b^\dagger b}^{(-1)}| \cos(\delta t - \phi), \quad (37)$$

where we have written the complex number $\Xi_{b^\dagger b}^{(-1)}$ in terms of its absolute value and phase ϕ [14]. Note that Eq. (37) is the squared width in x -direction of an ellipse with major and minor axis $\langle X_\pm^2 \rangle^{1/2}$, rotating at frequency $\delta/2$, with an initial tilt of $\phi/2$. This is no coincidence—the Wigner density of a squeezed state is an ellipse. There is one frame in which it is

stationary, whereas in all other frames, the ellipse is rotating, and thus a measurement of the variance will return an average over both quadratures. Note that rotating the ellipse by π maps it onto itself, so we can take $\vartheta \in [0, \pi)$.

The conclusion is that in order to detect the squeezing we have to follow the quadrature and make the measurement in a special rotating frame. The necessity to “follow” the quadrature has been mentioned in the discussion of QND measurements in Ref. [9]. The fact that we need to measure the rotating spectrum components to observe squeezing substantiates the claim that essential information can be hidden in rotating components of spectra. In the literature, this special case is what characterizes a so-called “phase-sensitive” detector, also called “phase nonpreserving amplifier” in Ref. [9]. Such a detector requires an external “clock” (here the beating of the laser drives) in order to keep track of the rotating quadrature, as noted in Ref. [15].

In Fig. 2 we illustrate how these concepts take form on the level of the mechanical spectra and plot the physical spectrum $S_{X_\nu^\vartheta X_\nu^\vartheta}^{(0)}(\omega)$ in the three most relevant cases. The first panel corresponds to $\nu = 0 = \vartheta$, i.e. the spectrum of the lab frame position quadrature $X_0^0 = x = b + b^\dagger$. The left and right peak correspond to contributions of $\langle b^\dagger b \rangle$ and $\langle bb^\dagger \rangle$, respectively. The absolute value of the rotating terms is shown as well. In general, they are complex, with a phase depending on t and ϑ .

The second and third panel in Fig. 2 are the spectra in the special rotating frame $\nu = \delta/2$. The first consequence of going into a rotating frame is that the peaks are displaced (not unilaterally, because b and b^\dagger get opposite phases, see Eq. (18)). In this frame, all peaks end up on top of each other. Equation (14) ensures that the imaginary parts of the rotating Fourier components cancel, while their relative angle in the complex plane is 2ϑ . We show the two cases in which they (individually) are entirely real, $\vartheta = 0, \pi/2$, and thus have the strongest effect. $\vartheta = 0, \pi/2$ corresponds to the squeezed and antisqueezed quadrature X_\mp (second and third panel), with

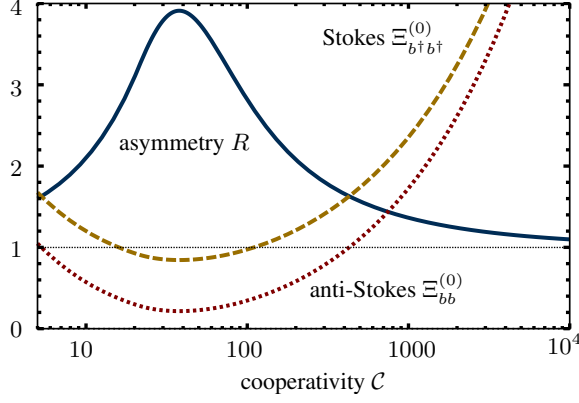


FIG. 3. **Sideband asymmetry.** Weights of the left and the right peak of the mechanical spectrum $S_{xx}^{(0)}$ in the lab frame as a function of cooperativity \mathcal{C} . Left peak weight $\Xi_{bb}^{(0)}$ is labelled anti-Stokes (red dotted), right peak weight $\Xi_{b^\dagger b^\dagger}^{(0)}$ is labelled Stokes (yellow dashed). Blue (solid) is their ratio $R = \Xi_{b^\dagger b^\dagger}^{(0)}/\Xi_{bb}^{(0)}$. Parameters are $\gamma/\kappa = 10^{-4}$, $n_{\text{th}} = 10$, $\Delta = -\Omega$, $\delta = 2\Omega$. Ω/κ is irrelevant in RWA.

the smallest and largest variance, respectively.

C. Squeezing for exact sideband driving

Reference [5] considered the case where the drives are on the sidebands, i.e., $\delta = 2\Omega$ and $\Delta = -\Omega$. Within RWA, the physical spectrum (cf. Eq. (20)) of the squeezed quadrature in a frame rotating with the mechanical frequency Ω is given by

$$S_{X_\Omega^0 X_\Omega^0}(\omega) = \frac{\kappa |\chi_c(\omega + \Omega)|^2 (G_- - G_+)^2 + \gamma(2n_{\text{th}} + 1)}{|\chi_m^{-1}(\omega + \Omega) + \chi_c(\omega + \Omega)\mathcal{G}^2|^2}. \quad (38)$$

This is a roundabout way to arrive at the desired result, as in this case it is easier to directly solve Eqs. (4a) and (4b) in a rotating frame, but our method is more general, enabling general detunings, rotating frames, and even beyond-RWA numerics.

Integrating Eq. (38) over frequency, we obtain the variance of the squeezed and antisqueezed quadratures

$$\langle X_\pm^2 \rangle = \frac{1}{\kappa + \gamma} \left[(2n_{\text{th}} + 1)\gamma \left(1 + \frac{\kappa}{\gamma + 4\mathcal{G}^2/\kappa} \right) + \frac{4(G_- \pm G_+)^2}{\gamma + 4\mathcal{G}^2/\kappa} \right], \quad (39)$$

where $X_- = X_{\nu=\Omega}^{\vartheta=0}$ and $X_+ = X_{\nu=\Omega}^{\vartheta=\pi/2}$. The result agrees with Ref. [1], where $(\kappa + \gamma)^{-1} \approx \kappa^{-1}$ was approximated.

Within our framework it is straightforward to find out how squeezing looks like in the lab frame. In Fig. 2(a) we plot the

spectrum of the lab frame position operator $X_0^0 = x = b + b^\dagger$

$$S_{xx}^{(0)}(\omega) = \frac{(n_{\text{th}} + 1)\gamma + \kappa\mathcal{G}_-^2 |\chi_c(\omega)|^2}{|\chi_m^{-1}(\omega) + \chi_c(\omega)\mathcal{G}^2|^2} + \frac{\gamma n_{\text{th}} + \kappa\mathcal{G}_+^2 |\chi_c(-\omega)|^2}{|\chi_m^{-1}(-\omega) + \chi_c(-\omega)\mathcal{G}^2|^2}. \quad (40)$$

It has two peaks as long as we do not consider the strong-coupling regime, where normal-mode splitting occurs. We call them Stokes ($\omega = \Omega$) and anti-Stokes ($\omega = -\Omega$) [7]. As we have discussed, the squeezing terms are not present.

The weights of the left and right (anti-Stokes and Stokes) peak are the integrals $\Xi_{bb}^{(0)}$ and $\Xi_{b^\dagger b^\dagger}^{(0)}$, respectively. Ξ is defined in Eq. (34). The ratio of Stokes to anti-Stokes is the asymmetry $R = \Xi_{b^\dagger b^\dagger}^{(0)}/\Xi_{bb}^{(0)}$. In Fig. 3 we plot the weights as a function of cooperativity \mathcal{C} for the ‘‘optimal driving strength’’ as defined in Ref. [5]

$$G_- = \sqrt{\frac{\mathcal{C}\kappa\gamma}{4}}, \quad G_+ = G_- \left(1 - \sqrt{\frac{1 + 2n_{\text{th}}}{\mathcal{C}}} \right). \quad (41)$$

At low cooperativities, the asymmetry increases with cooperativity. Physically, this is because the system is cooled. However, as the coupling strength is increased further, the asymmetry decreases and approaches unity. This is due to the fact that dissipative squeezing leads to a squeezed, thermal state with an effective temperature that increases with the degree of squeezing. In the lab frame, the squeezing terms are not a part of the spectrum, so we expect that the quadrature variance and the weight of both peaks increase. This leads to a decrease in the asymmetry R as a function of cooperativity \mathcal{C} .

D. Squeezing loss due to detuning

Instead of having both drives exactly on the sidebands as in Sec. III C, in this section we will study the behavior of the system when the drives are detuned from the sidebands. Here, we will only analyze the case $\Delta = -\Omega$, $\delta = 2\Omega + \varepsilon$, i.e., the red drive remains on the sideband. Changing the detuning of the cooling drive will lead to an instability for $G_+ > \gamma$.

In Fig. 4, we plot the variance of the two quadratures, their average $2\langle b^\dagger b \rangle + 1$, and the weak-coupling result for the variance of the squeezed quadrature $\langle X_- \rangle$ as a function of the detuning ε . There are two scales on which effects occur [16].

The larger scale is the cavity mode dissipation rate κ . Detunings on this scale render the detuned drive ineffective such that only cooling remains. In particular, we see that the occupation and the variance of both quadratures decreases, as the influence of the blue drive becomes weaker. Note that by this point both quadrature variances are already almost equal.

The smaller scale is the effective mechanical damping $\tilde{\gamma} = \gamma + 4\mathcal{G}^2/\kappa$, introduced in Sec. III A. For $\varepsilon \sim \tilde{\gamma}$, squeezing has disappeared and for strong driving an instability occurs, see Sec. III E. In Fig. 4 the loss of squeezing is evidenced by the two quadrature variances becoming equal. On this scale it does not matter whether we move the blue drive away or

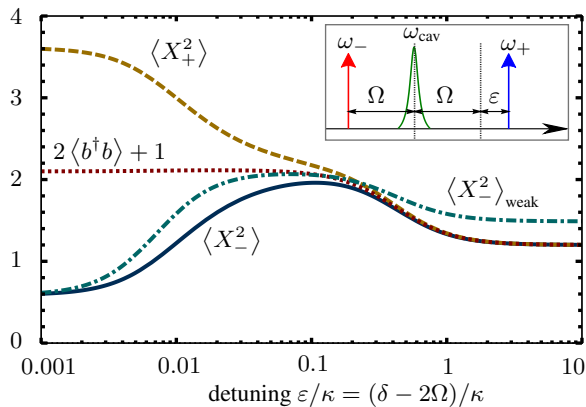


FIG. 4. **Squeezing loss due to detuning.** Blue (solid) is the variance of the squeezed quadrature $\langle X_-^2 \rangle$, orange (dashed) the antisqueezed quadrature $\langle X_+^2 \rangle$, and red (dotted) is $2\langle b^\dagger b \rangle + 1$ as a function of detuning of the blue drive $\varepsilon = \delta - 2\Omega$. They have been obtained from Eq. (36). We also show the weak-coupling result Eq. (32) for the squeezed quadrature in turquoise (dash-dotted). The inset shows the driving scheme with the two driving frequencies ω_\pm relative to the cavity frequency ω_{cav} . Parameters are $\gamma/\kappa = 10^{-4}$, $n_{\text{th}} = 10$, $\mathcal{C} = 10^2$, $\Delta = -\Omega$, so that $\tilde{\gamma} \approx 0.02\kappa$. Ω/κ is irrelevant in RWA.

the red, as long as $\varepsilon \ll \kappa$, as these effects are due to the mismatch between the beating frequency of the two lasers δ and the mechanical frequency Ω . The beating can be thought of as a stroboscopic measurement of one of the quadratures every half period, akin to the scheme in Ref. [17]. For finite detuning ε the measured quadrature starts to rotate at frequency $\varepsilon/2$ with respect to mechanical quadrature, so $2/\varepsilon$ is the timescale on which the squeezed and antisqueezed quadratures mix and interchange, see Eq. (28). In this sense, we are probing dynamical effects—they only become visible if their timescale is comparable to ε^{-1} . The mixing eventually mitigates squeezing entirely at $\varepsilon \sim \tilde{\gamma}$, i.e., when the mixing rate balances the squeezing rate as predicted in the weak-coupling approximation (32). The weak-coupling approximation (32) does not correctly capture the sideband cooling limit, the noise added by the blue-detuned drive does not vanish in the limit $\varepsilon \rightarrow \infty$, as discussed below Eq. (32).

E. Heating and parametric instability

We now turn to the strong-coupling effects. If the system is coupled more strongly, with \mathcal{G} approaching κ , the minimum variance of the squeezed quadrature saturates at the lower bound $\langle X_-^2 \rangle \rightarrow \gamma(1 + 2n_{\text{th}})/(\kappa + \gamma)$, see Eq. (39) or Ref. [5]. In this regime, moving one of the lasers away from the sidebands, i.e., $\delta \neq 2\Omega$, will result in a heating effect, and an instability for very strong coupling, see Fig. 5 and Appendix F.

In Fig. 5, we plot the squeezed quadrature variance $\langle X_-^2 \rangle$ as a function of the detuning of the blue laser ε for cooperativities $\mathcal{C} = 50, 500, 2000$. As we couple more strongly, heating occurs in addition to squeezing loss. From $\varepsilon = 0$, and

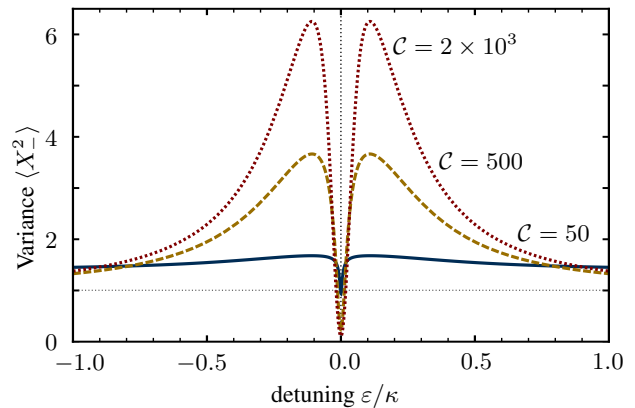


FIG. 5. **Heating due to detuning.** Blue (solid), yellow (dashed), and red (dotted) are the squeezed quadrature variances $\langle X_-^2 \rangle$ for cooperativities $\mathcal{C} = 50, 500, 2000$ as a function of detuning ε/κ . Here, $\gamma/\kappa = 10^{-4}$, $n_{\text{th}} = 10$, $\Delta = -\Omega$. Ω/κ is irrelevant in RWA.

for large enough \mathcal{C} , the squeezed quadrature variance first increases steeply, reaches a peak, and then decreases. The peak corresponds to the point where the system is closest to instability, whereas the decay for $\varepsilon \sim \kappa$ is the convergence to usual sideband cooling, as mentioned before. The heating effect has been mentioned in Ref. [2] where it was used to tune the lasers to the mechanical sidebands. Again, we find the separation of time scales: squeezing loss and heating for $\varepsilon \sim \tilde{\gamma}$ and cooling for $\varepsilon \sim \kappa$. We analyze the instability further in Appendix F.

IV. MEASUREMENT WITH SECOND CAVITY MODE

The ideas introduced above can be nicely illustrated if we study how the mechanical spectrum can be observed through a second, weakly coupled “readout” mode. Our approach will be the same as above, with two lasers pumping a single cavity mode, except that in this section the mechanical oscillator is a black-box with a fixed, unknown spectrum that we would like to measure. We will neglect the measurement backaction on the mechanical oscillator, an assumption that is excellent for QND measurements and reasonable for weak coupling.

Analogous to the first cavity mode \hat{d} , the linearized quantum Langevin equation for the second cavity mode \hat{d}_2 is

$$\dot{d}_2 = \left(i\Delta_2 - \frac{\kappa_2}{2} \right) d_2 + \sqrt{\kappa_2} d_{2\text{in}} + i(G_{2+} e^{-i\delta_2 t} + G_{2-})(b^\dagger + b), \quad (42)$$

where $\Delta_2 = \omega_{2-} - \omega_{\text{cav},2}$ is the detuning of the lower frequency laser from the frequency of the second cavity mode, $\delta_2 = \omega_{2+} - \omega_{2-}$ is the frequency difference between the blue and the red drive on the second cavity mode, κ_2 the dissipation rate of the second cavity mode, and $G_{2\pm}$ are the enhanced optomechanical couplings, see Fig. 1.

We can apply an analysis as above to find the most general spectra measured through the second cavity mode. For details,

we refer to Appendix H. We split Eq. (42) up into Fourier components of the two frequencies present

$$d_2(t) = \sum_{n,m} e^{in\delta t + im\delta_2 t} d_2^{(m,n)}(t). \quad (43)$$

Generalized to two frequencies, the stationary spectrum is

$$\begin{aligned} S_{d_2^\dagger d_2}^{(0)}(\omega) \\ = \sum_{n,m} \int \frac{d\omega'}{2\pi} \left\langle d_2^{(n,m)\dagger}(\omega + n\delta + m\delta_2) d_2^{(-n,-m)}(\omega') \right\rangle. \end{aligned} \quad (44)$$

If $\delta \neq \delta_2$ (and are not multiples of each other), b does not have any components commensurate with δ_2 , and hence

$$b^{(n,m)} = 0, \quad \forall m \neq 0. \quad (45)$$

The stationary part simplifies to

$$S_{d_2^\dagger d_2}^{(0)}(\omega) = |\chi_2(-\omega)|^2 \left[G_{2-}^2 S_{xx}^{(0)}(\omega) + G_{2+}^2 S_{xx}^{(0)}(\omega + \delta_2) \right]. \quad (46)$$

$x = X_0^0$ here, as always, refers to the non-rotating position quadrature in the lab frame. Therefore, the only effect of having a second drive is that now there are two copies of the mechanical spectrum superposed with a different weights and shifted by δ_2 relative to each other. Furthermore, both are filtered by the response function of the cavity mode $\chi_2(\omega) = [\kappa_2/2 - i(\omega + \Delta_2)]^{-1}$. This case corresponds to the ‘‘non-QND’’ measurement in Ref. [3]. It is an average over the squeezed and antisqueezed quadrature, see Sec. III B and Fig. 2.

A special case is $\delta_2 = \delta$, in which Eq. (45) does not hold. Instead, we find for the stationary part of the d_2 spectrum

$$\begin{aligned} S_{d_2^\dagger d_2}^{(0)}(\omega) = |\chi_2(-\omega)|^2 \left\{ G_{2-}^2 S_{xx}^{(0)}(\omega) + G_{2+}^2 S_{xx}^{(0)}(\omega + \delta) \right. \\ \left. + G_{2-} G_{2+} \left[S_{xx}^{(-1)}(\omega + \delta) + S_{xx}^{(1)}(\omega) \right] \right\}. \end{aligned} \quad (47)$$

Note that here the rotating parts of S_{xx} contribute to $S_{d_2^\dagger d_2}^{(0)}$.

In RWA, only $b^{(0)}$, $b^{(0)\dagger}$, $b^{(-1)}$, $b^{(1)\dagger}$ are non-zero. Depending on the cavity linewidth κ_2 , the prefactor $|\chi_2(-\omega)|^2$ more or less sharply picks out the contribution at $\omega = -\Delta_2$. This causes a suppression of counterrotating terms. So, if we make the readout mode a good cavity with $\kappa_2 \ll \Omega$ and choose $\Delta_2 = -\delta/2$, then we can make a second RWA (this time for the second optical mode) and we are left with

$$\begin{aligned} S_{d_2^\dagger d_2}^{(0)}(\omega) = |\chi_2(-\omega)|^2 \left[G_{2-}^2 S_{b^\dagger b}^{(0)}(\omega) + G_{2+}^2 S_{bb^\dagger}^{(0)}(\omega + \delta) \right. \\ \left. + G_{2+} G_{2-} (S_{bb}^{(-1)}(\omega + \delta) + S_{b^\dagger b^\dagger}^{(1)}(\omega)) \right] \\ = |\chi_2(-\omega)|^2 G_2^2 S_{X_{\delta/2}^0 X_{\delta/2}^0}(\omega + \delta/2), \end{aligned} \quad (48)$$

where in the last line we have chosen $G_{2+} = G_{2-} \equiv G_2$, and identified the physical spectrum (20). Thus, this is a measurement of a rotating quadrature. In order to find out which terms

contribute in (48), it is helpful to refer to the plot of spectrum Fourier components in RWA shown in Fig. 2, and remember that $|\chi_2(-\omega)|^2$ picks out contributions around $\omega = -\delta/2$. If additionally $\delta = 2\Omega$, this measurement is QND, as in Ref. [3].

V. CONCLUSION

In this article we presented a framework to deal with time-periodic quantum Langevin equations that builds on Floquet theory. Since the steady-state solution is periodic, it amounts to splitting system operators up into their Fourier components (5). The spectrum Fourier components (12) can be used to calculate power spectra in any rotating frame (18). This opens a new perspective to understand the relation between the measured spectra and rotating frames, as discussed in Sec. II C.

We exemplify the new tool by studying a bichromatically driven cavity optomechanical system that has garnered a large amount of interest recently [1–3]. This setting has been used to prepare a mechanical oscillator in a quantum-squeezed state, following the proposal [5]. Using the full analytical solution in the rotating-wave approximation, we shed light on the squeezing mechanism and provide some intuition for the behavior of bichromatically driven systems (Sec. III).

Looking ahead, the presented framework can be used to map time-periodic quantum Langevin equations to familiar, coupled, stationary ones, albeit—as usual for Floquet methods—infinite many such equations. Where an exact analytical solution is not feasible, an approximation can be found by truncating the infinite matrix (10). We would like to point out Ref. [18] as a graphical tool to approximate the inverses of matrices such as Eq. (10), to any desired order in the coupling. Furthermore, it may prove beneficial to identify conditions under which exact solutions can be found.

ACKNOWLEDGMENTS

We are grateful to Aashish Clerk, Florian Marquardt, Amir Safavi-Naeini, John Teufel, and, in particular, Tobias Kippenberg for stimulating and insightful discussions. A.N. holds a University Research Fellowship from the Royal Society and acknowledges additional support from the Winton Programme for the Physics of Sustainability. D.M. is supported by an EPSRC studentship.

Appendix A: Floquet engineering

In the case studied in the main text, the infinite matrix (10) only contains $A^{(0)}$, $A^{(\pm 1)}$, the others being zero. We describe how to activate more blocks and their general structure below.

One can think of $A^{(0)}$ as the fundamental building block and of $A^{(\pm n)}$ for $n > 0$ as contributions that oscillate with $n\delta$ and therefore are capable of coupling fundamental blocks a distance n away from each other.

Any periodic driving with period $T = 2\pi/\delta$, either due to anharmonic drives or several harmonic ones, can be expressed

as a Fourier series with fundamental frequency δ . Usually, the drive frequencies are offset by the cavity mode frequency and some detuning, i.e.,

$$\omega_n = \omega_{\text{cav}} + \Delta + in\delta. \quad (\text{A1})$$

It is useful to define the matrices, see Eqs. (9b) and (9c),

$$A_+ \equiv \left(\begin{array}{c|c} 1 & \\ \hline -1 & -1 \end{array} \right), \quad A_- \equiv \left(\begin{array}{c|c} 1 & 1 \\ \hline & -1 \end{array} \right). \quad (\text{A2})$$

If we assume a driving Hamiltonian of the form

$$H_{\text{drive}} = e^{-i(\omega_{\text{cav}} + \Delta)t} \left(\sum_n \alpha_n e^{-in\delta t} \right) \hat{a}^\dagger + \text{h.c.}, \quad (\text{A3})$$

we can linearize the Hamiltonian by a displacement operation like the one used in the main text, with

$$\hat{a} = e^{-i(\omega_{\text{cav}} + \Delta)t} \left(\sum_n \bar{a}_n e^{-in\delta t} + \hat{d} \right). \quad (\text{A4})$$

Defining $J_n = \bar{a}_n g$, the enhanced optomechanical coupling strengths, we can write

$$A^{(n)} = iJ_n A_+ + iJ_{-n} A_- - \delta_{n,0} M_0, \quad (\text{A5})$$

where

$$M_0 \equiv \begin{pmatrix} \frac{\kappa}{2} - i\Delta & & & \\ & \frac{\gamma}{2} + i\Omega & & \\ & & \frac{\kappa}{2} + i\Delta & \\ & & & \frac{\gamma}{2} - i\Omega \end{pmatrix}. \quad (\text{A6})$$

This includes the case discussed in the main text (9) and provides a simple recipe to couple any two blocks together and thus to engineer new types of driving schemes. Moreover, it is straightforward to adapt this to a different system, once the relevant matrices M_0, A_\pm have been identified.

Appendix B: The Fourier transform of the stationary part of the autocorrelator is the measured spectrum

We use the definition for the spectral density from Ref. [9] (see also [19, 20], where the same definition is used, also in the context of squeezing)

$$\begin{aligned} S_{A^\dagger A}^{\text{power}}[\omega] &\equiv \lim_{T \rightarrow \infty} \langle |A_T[\omega]|^2 \rangle \\ &= \lim_{T \rightarrow \infty} \frac{1}{T} \int_0^T \int_0^T dt dt' e^{i\omega(t'-t)} \\ &\quad \times \sum_{n,m} e^{in\delta t' + im\delta t} \langle A^{(n)\dagger}(t') A^{(m)}(t) \rangle \\ &= \lim_{T \rightarrow \infty} \frac{1}{T} \int_0^T dt \int_{-t}^{T-t} d\tau e^{i\omega\tau} \\ &\quad \times \sum_{n,m} e^{i\delta[(n+m)t + n\tau]} \langle A^{(n)\dagger}(t + \tau) A^{(m)}(t) \rangle. \end{aligned} \quad (\text{B1})$$

The expectation value in the last line is in fact time-translation invariant and hence independent of t . Furthermore, as $T \rightarrow \infty$, the second integral becomes $\int_{-\infty}^{\infty}$. Therefore, the expression splits into two parts

$$\begin{aligned} S_{A^\dagger A}^{\text{power}}[\omega] &= \sum_n \left(\lim_{T \rightarrow \infty} \frac{1}{T} \int_0^T dt \sum_m e^{i\delta(n+m)t} \right) \\ &\quad \times \left(\int_{-\infty}^{\infty} d\tau e^{i\delta n\tau + i\omega\tau} \langle A^{(n)\dagger}(\tau) A^{(m)}(0) \rangle \right) \\ &= \sum_{n,m} \delta_{n,-m} f_{A^\dagger A}(n, m, \omega + n\delta) = S_{A^\dagger A}^{(0)}(\omega). \end{aligned} \quad (\text{B2})$$

Where it is helpful to be more precise, we note that the visibility of rotating terms at frequency ω will decrease as $\text{sinc}(\omega T/2)$, where T is the total measurement time.

Appendix C: Properties of the spectrum Fourier components

Let A be governed by a time-periodic Langevin equation. Each of its Fourier components $A^{(n)}$ obeys a Langevin equation without explicit time-dependence. If the system assumes a stationary state (which it does if all eigenvalues of the Langevin matrix have negative real part), we can write the Fourier transformed Fourier components as a linear combination of the N input operators $\{F_{i,\text{in}}(\omega)\}$ (this set contains input operators and their hermitian conjugates)

$$A^{(n)}(\omega) = \sum_i K_i^{(n)}(\omega) F_{i,\text{in}}(\omega), \quad (\text{C1})$$

where $\mathbf{K}^{(n)}(\omega)$ is an N -component vector (for each Fourier component n) containing the appropriate functions. In the convention for Fourier transforms described in the main text (Eq. (5)), the hermitian conjugate of this equation gives

$$A^{(n)\dagger}(\omega) = \sum_i K_i^{(-n)*}(-\omega) F_{i,\text{in}}^\dagger(\omega). \quad (\text{C2})$$

The stationary part of the spectrum is (cf. Eq. (13))

$$\begin{aligned} S_{A^\dagger A}^{(0)}(\omega) &= \sum_n \int \frac{d\omega'}{2\pi} \langle A^{(n)\dagger}(\omega + n\delta) A^{(-n)}(\omega') \rangle \\ &= \sum_{n,i,j} \int \frac{d\omega'}{2\pi} K_i^{(-n)*}(-\omega - n\delta) K_j^{(-n)}(\omega') \\ &\quad \times \langle F_{i,\text{in}}^\dagger(\omega + n\delta) F_{j,\text{in}}(\omega') \rangle \\ &= \sum_{n,i} n_i K_i^{(-n)*}(-\omega - n\delta) K_i^{(-n)}(-\omega - n\delta) \\ &= \sum_{n,i} n_i \left| K_i^{(-n)}(-\omega - n\delta) \right|^2, \end{aligned} \quad (\text{C3})$$

where we had to assume the noise correlators

$$\langle F_{i,\text{in}}^\dagger(\omega) F_{j,\text{in}}(\omega') \rangle = 2\pi n_i \delta_{ij} \delta(\omega + \omega'), \quad (\text{C4})$$

with thermal occupations $n_i \geq 0$. Thus the stationary part is real and positive.

Another property is $[S_{A^\dagger B}^{(n)}(\omega)]^\dagger = S_{B^\dagger A}^{(-n)}(\omega + n\delta)$. The proof is by expansion

$$\begin{aligned}
& [S_{A^\dagger B}^{(n)}(\omega)]^\dagger \\
&= \left[\sum_m \int \frac{d\omega'}{2\pi} \langle A^{(m)\dagger}(\omega + m\delta) B^{(n-m)}(\omega') \rangle \right]^\dagger \\
&= \sum_m \int \frac{d\omega'}{2\pi} \langle B^{(m-n)\dagger}(-\omega') A^{(-m)}(-\omega - m\delta) \rangle \\
&= \sum_m \int \frac{d\omega'}{2\pi} 2\pi\delta(-\omega - m\delta - \omega') \\
&\quad \times f_{B^\dagger A}(m - n, -m, -\omega - m\delta) \\
&= \sum_m \int \frac{d\omega'}{2\pi} 2\pi\delta(\omega' + \omega + (m + n)\delta) \\
&\quad \times f_{B^\dagger A}(m, -m - n, \omega') \\
&= \sum_m \int \frac{d\omega'}{2\pi} \langle B^{(m)\dagger}(\omega + (m + n)\delta) A^{(-m-n)}(\omega') \rangle \\
&= S_{B^\dagger A}^{(-n)}(\omega + n\delta), \tag{C5}
\end{aligned}$$

where for convenience we have again used the shorthand (19)

$$f_{A^\dagger B}(n, m, \omega) \equiv \int \frac{d\omega'}{2\pi} \langle A^{(n)\dagger}(\omega) B^{(m)}(\omega') \rangle, \tag{C6}$$

which assumes noise correlators of the form (C4).

Appendix D: Full solution to bichromatically driven optomechanical system in RWA

In RWA, the infinite set of differential equations (7) decouples into sets of four. The blocks disconnected from input operators will decay and vanish in the steady state. Thus only two blocks (mutually hermitian conjugates) are non-zero. The problem reduces to solving

$$\begin{aligned}
& \begin{pmatrix} \chi_c^{-1}(\omega) & -iG_- & 0 & -iG_+ \\ -iG_- & \chi_m^{-1}(\omega) & -iG_+ & 0 \\ 0 & iG_+ & \chi_c^{-1*}(-\omega + \delta) & iG_- \\ iG_+ & 0 & iG_- & \chi_m^{-1*}(-\omega + \delta) \end{pmatrix} \\
& \times \begin{pmatrix} d^{(0)}(\omega) \\ b^{(0)}(\omega) \\ d^{(1)\dagger}(\omega) \\ b^{(1)\dagger}(\omega) \end{pmatrix} = \begin{pmatrix} \sqrt{\kappa} d_{\text{in}}(\omega) \\ \sqrt{\gamma} b_{\text{in}}(\omega) \\ 0 \\ 0 \end{pmatrix}, \tag{D1}
\end{aligned}$$

with the cavity and mechanical response functions $\chi_c^{-1}(\omega) = \kappa/2 - i(\omega + \Delta)$ and $\chi_m^{-1}(\omega) = \gamma/2 - i(\omega - \Omega)$, respectively.

Eliminating the light field we find

$$\begin{aligned}
& \begin{pmatrix} \chi_m^{-1}(\omega) - i\Sigma_{00}(\omega) & -i\Sigma_{01}(\omega) \\ i\Sigma_{01}^*(-\omega + \delta) & \chi_m^{-1*}(-\omega + \delta) + i\Sigma_{00}^*(-\omega + \delta) \end{pmatrix} \\
& \times \begin{pmatrix} b^{(0)} \\ b^{(1)\dagger} \end{pmatrix} = \begin{pmatrix} \sqrt{\gamma} & iG_- \sqrt{\kappa} \chi_c(\omega) \\ 0 & -iG_+ \sqrt{\kappa} \chi_c(\omega) \end{pmatrix} \begin{pmatrix} b_{\text{in}} \\ d_{\text{in}} \end{pmatrix}, \tag{D2}
\end{aligned}$$

with

$$\begin{aligned}
\Sigma_{00}(\omega) &= i[G_-^2 \chi_c(\omega) - G_+^2 \chi_c^*(-\omega + \delta)], \\
\Sigma_{01}(\omega) &= iG_- G_+ [\chi_c(\omega) - \chi_c^*(-\omega + \delta)]. \tag{D3}
\end{aligned}$$

This allows us to write the system operators in terms of input operators

$$\begin{pmatrix} b^{(0)}(\omega) \\ b^{(1)\dagger}(\omega) \end{pmatrix} = \begin{pmatrix} a(\omega) & c(\omega) \\ f(\omega) & g(\omega) \end{pmatrix} \begin{pmatrix} b_{\text{in}}(\omega) \\ d_{\text{in}}(\omega) \end{pmatrix}, \tag{D4}$$

with

$$a(\omega) = A^{-1}(\omega) \sqrt{\gamma} [\chi_m^{-1*}(-\omega + \delta) + i\Sigma_{00}^*(-\omega + \delta)], \tag{D5a}$$

$$c(\omega) = iA^{-1}(\omega) \sqrt{\kappa} \chi_c(\omega) G_- \times [\chi_m^{-1*}(-\omega + \delta) + \mathcal{G}^2 \chi_c^*(-\omega + \delta)], \tag{D5b}$$

$$f(\omega) = -iA^{-1}(\omega) \sqrt{\gamma} \Sigma_{01}(\omega), \tag{D5c}$$

$$g(\omega) = -iA^{-1}(\omega) \sqrt{\kappa} \chi_c(\omega) G_+ \times [\chi_m^{-1}(\omega) + \mathcal{G}^2 \chi_c^*(-\omega + \delta)], \tag{D5d}$$

where $\mathcal{G}^2 \equiv G_-^2 - G_+^2$ and $A(\omega)$ is the determinant of the matrix on the left hand side of Eq. (D2),

$$\begin{aligned}
A(\omega) &= [\chi_m^{-1*}(-\omega + \delta) + i\Sigma_{00}^*(-\omega + \delta)] \\
&\times [\chi_m^{-1}(\omega) - i\Sigma_{00}(\omega)] - \Sigma_{01}(\omega) \Sigma_{01}^*(-\omega + \delta). \tag{D6}
\end{aligned}$$

The analytical solution can be used to find spectrum Fourier components, employing Eq. (13),

$$S_{b^\dagger b}^{(0)}(\omega) = |a(-\omega)|^2 n_{\text{th}} + |f(\omega + \delta)|^2 (n_{\text{th}} + 1) + |g(\omega + \delta)|^2, \tag{D7a}$$

$$S_{bb^\dagger}^{(0)}(\omega) = (n_{\text{th}} + 1) |a(\omega)|^2 + |c(\omega)|^2 + n_{\text{th}} |f(-\omega + \delta)|^2, \tag{D7b}$$

$$S_{xx}^{(0)}(\omega) = (n_{\text{th}} + 1) (|a(\omega)|^2 + |f(\omega + \delta)|^2) + |c(\omega)|^2 + n_{\text{th}} (|a(-\omega)|^2 + |f(-\omega + \delta)|^2) + |g(\omega + \delta)|^2, \tag{D7c}$$

$$\begin{aligned}
S_{bb}^{(-1)}(\omega) &= (n_{\text{th}} + 1) a(\omega) f^*(\omega) + c(\omega) g^*(\omega) \\
&\quad + n_{\text{th}} f^*(-\omega + \delta) a(-\omega + \delta) \\
&= [S_{b^\dagger b^\dagger}^{(1)}(\omega - \delta)]^\dagger. \tag{D7d}
\end{aligned}$$

An important special case [2, 3] is the symmetric detuning $\delta = 2\Omega + \varepsilon$, $\Delta = -\Omega - \varepsilon/2 = -\delta/2$. Crucially, this leads to $\chi_c^*(-\omega + \delta) = \chi_c(\omega)$, which implies

$$\Sigma_{00} = i\chi_c(\omega) \mathcal{G}^2, \quad \Sigma_{01} = 0. \tag{D8}$$

Thus, the determinant $A(\omega)$ takes a particularly simple form

$$A(\omega) = [\chi_m^{-1}(\omega - \varepsilon) + \chi_c(\omega)\mathcal{G}^2] [\chi_m^{-1}(\omega) + \chi_c(\omega)\mathcal{G}^2] \quad (\text{D9})$$

and so do the auxiliary functions

$$\begin{aligned} a(\omega) &= \sqrt{\gamma} / [\chi_m^{-1}(\omega) + \chi_c(\omega)\mathcal{G}^2], \\ c(\omega) &= i\sqrt{\kappa}G_- \chi_c(\omega) / [\chi_m^{-1}(\omega) + \chi_c(\omega)\mathcal{G}^2], \\ f(\omega) &= 0, \\ g(\omega) &= -i\sqrt{\kappa}\chi_c(\omega)G_+ / [\chi_m^{-1}(\omega - \varepsilon) + \mathcal{G}^2\chi_c(\omega)]. \end{aligned} \quad (\text{D10})$$

And the spectra are

$$S_{xx}^{(0)}(\omega) = \frac{(n_{\text{th}} + 1)\gamma + \kappa G_-^2 |\chi_c(\omega)|^2}{|\chi_m^{-1}(\omega) + \chi_c(\omega)\mathcal{G}^2|^2} + \frac{\gamma n_{\text{th}} + \kappa G_+^2 |\chi_c(-\omega)|^2}{|\chi_m^{-1}(-\omega) + \chi_c(-\omega)\mathcal{G}^2|^2}, \quad (\text{D11a})$$

$$\begin{aligned} S_{xx}^{(1)}(\omega) &= \frac{\kappa G_- G_+ \chi_c(-\omega)}{\sigma^*(-\omega) [\chi_m^{-1}(-\omega - \varepsilon) + \chi_c(-\omega)\mathcal{G}^2]} \\ &= [S_{xx}^{(-1)}(-\omega)]^*, \end{aligned} \quad (\text{D11b})$$

where we have introduced $\sigma(\omega) = \mathcal{G}^2 + \chi_m^{-1}(\omega)\chi_c^{-1}(\omega)$.

We can employ Eq. (20) for the physical spectrum in the special rotating frame. It has two parts. One is the previously stationary part, which corresponds to the radially symmetric contribution to the Wigner density (and therefore it remains stationary, despite going into a rotating frame)

$$\begin{aligned} U(\omega) &= S_{b^\dagger b}^{(0)}(\omega - \delta/2) + S_{bb^\dagger}^{(0)}(\omega + \delta/2) \\ &= \kappa \left[\frac{G_-^2}{|\sigma(\omega + \delta/2)|^2} + \frac{G_+^2}{|\sigma(-\omega + \delta/2)|^2} \right] \\ &\quad + \frac{\gamma}{|\chi_c(\omega + \delta/2)|^2} \left[\frac{n_{\text{th}} + 1}{|\sigma(\omega + \delta/2)|^2} + \frac{n_{\text{th}}}{|\sigma(-\omega + \delta/2)|^2} \right] \end{aligned} \quad (\text{D12})$$

The other one stems from the previously rotating parts

$$\begin{aligned} V(\omega) &= S_{b^\dagger b^\dagger}^{(1)}(\omega - \delta/2) + S_{bb}^{(-1)}(\omega + \delta/2) \\ &= -2\kappa G_- G_+ \\ &\quad \times \text{Re} \left\{ \frac{1}{|\sigma(\omega + \delta/2)|^2 - i\varepsilon \chi_c^{-1*}(\omega + \delta/2)\sigma(\omega + \delta/2)} \right\}. \end{aligned} \quad (\text{D13})$$

Finally,

$$S_{X_\mp X_\mp}(\omega) = U(\omega) \pm V(\omega). \quad (\text{D14})$$

Appendix E: Weak-coupling approximation to a bichromatically driven optomechanical system

Our approach in this section will be to perturb around the mechanical spectrum in the absence of coupling. We will do so up to second order in G_\pm .

The equations of motion in RWA (21), split up into Fourier components, are

$$\begin{aligned} \dot{d}^{(n)} &= \left(-in\delta + i\Delta - \frac{\kappa}{2} \right) d^{(n)} + \sqrt{\kappa}\delta_{n,0}d_{\text{in}} \\ &\quad + i \left(G_+ b^{(n+1)\dagger} + G_- b^{(n)} \right), \end{aligned} \quad (\text{E1a})$$

$$\begin{aligned} \dot{b}^{(n)} &= \left(-in\delta - i\Omega - \frac{\gamma}{2} \right) b^{(n)} + \sqrt{\gamma}\delta_{n,0}b_{\text{in}} \\ &\quad + i \left(G_+ d^{(n+1)\dagger} + G_- d^{(n)} \right). \end{aligned} \quad (\text{E1b})$$

The unperturbed mechanical spectrum consists only of $b^{(0)}$ and $b^{(0)\dagger}$. Thus, to first order,

$$d^{(0)}(\omega) = \chi_c(\omega) \left(\sqrt{\kappa}d_{\text{in}}(\omega) + iG_- b^{(0)}(\omega) \right), \quad (\text{E2a})$$

$$d^{(-1)}(\omega) = \chi_c(\omega + \delta) iG_+ b^{(0)\dagger}(\omega). \quad (\text{E2b})$$

We can now determine $b^{(0)}$ without knowledge of $b^{(-1)}$

$$\begin{aligned} \left(-i\omega + i\Omega + \frac{\gamma}{2} - G_+^2 \chi_c^*(-\omega + \delta) + G_-^2 \chi_c(\omega) \right) b^{(0)}(\omega) \\ = \sqrt{\gamma}b_{\text{in}}(\omega) + i\sqrt{\kappa}G_- \chi_c(\omega)d_{\text{in}}(\omega) + \mathcal{O}(G_\pm^3). \end{aligned} \quad (\text{E3})$$

The reason for this is that $b^{(-1)} = \mathcal{O}(G_\pm)$, such that the effect $b^{(-1)}$ has on $b^{(0)}$ (via the optical field) is at least $\mathcal{O}(G_\pm^3)$. The LHS of (E3) is the modified response function

$$\tilde{\chi}_m(\omega) = \left[\frac{\tilde{\gamma}(\omega)}{2} - i(\omega - \tilde{\Omega}(\omega)) \right]^{-1} \quad (\text{E4})$$

with

$$\tilde{\gamma}(\omega) = \gamma + \kappa (|\chi_c(\omega)|^2 G_-^2 - |\chi_c(-\omega + \delta)|^2 G_+^2), \quad (\text{E5a})$$

$$\begin{aligned} \tilde{\Omega}(\omega) &= \Omega + |\chi_c(\omega)|^2 (\omega + \Delta) G_-^2 \\ &\quad + |\chi_c(-\omega + \delta)|^2 (-\omega + \delta + \Delta) G_+^2. \end{aligned} \quad (\text{E5b})$$

The mechanical response function (E4) strongly suppresses contributions away from $\omega = -\tilde{\Omega} \approx -\Omega$. In comparison to χ_m , χ_c is flat (if $\tilde{\gamma} \ll \kappa$), such that we can approximate $\chi_c(\omega) \approx \chi_c(-\Omega)$. For $\Delta = -\Omega$ the corrections simplify to Eqs. (25a), and

$$b^{(0)}(\omega) = \tilde{\chi}_m(\omega) \sqrt{\gamma}b_{\text{in}} + \frac{2iG_-}{\sqrt{\kappa}} \chi_m(\omega)d_{\text{in}}. \quad (\text{E6})$$

We would like the same accuracy for the rotating components, so we keep the next order in d

$$\begin{aligned} d^{(0)}(\omega) &= \chi_c(\omega) \left(\sqrt{\kappa}d_{\text{in}}(\omega) + iG_- b^{(0)} + iG_+ b^{(1)\dagger}(\omega) \right), \\ d^{(-1)}(\omega) &= i\chi_c(\omega + \delta) \left(G_+ b^{(0)\dagger}(\omega) + G_- b^{(-1)}(\omega) \right). \end{aligned} \quad (\text{E7})$$

Then

$$\chi_m^{-1*}(-\omega + \delta)b^{(1)\dagger}(\omega) = -i \left(G_+ d^{(0)}(\omega) + G_- d^{(1)\dagger}(\omega) \right). \quad (\text{E8})$$

We substitute for d with Eq. (E7)

$$b^{(1)\dagger}(\omega) = \chi_m^*(-\omega + \delta) \left[-iG_+ \chi_c(\omega) \sqrt{\kappa} d_{\text{in}}(\omega) + G_+ G_- (\chi_c(\omega) - \chi_c^*(-\omega + \delta)) b^{(0)}(\omega) \right], \quad (\text{E9})$$

where $b^{(0)} = \chi_m(\omega) \sqrt{\gamma} b_{\text{in}}$ in the absence of driving (the second order corrections to $b^{(0)}$ would be fourth order in this equation). With a differently modified response function $\chi'_m = [\gamma'/2 - i(\omega - \Omega')^{-1}]^{-1}$, with

$$\gamma'(\omega) = \gamma + \kappa (|\chi_c(-\omega + \delta)|^2 G_-^2 - |\chi_c(\omega)|^2 G_+^2), \quad (\text{E10a})$$

$$\Omega'(\omega) = \Omega + |\chi_c(\omega)|^2 (\omega + \Delta) G_+^2 + |\chi_c(-\omega + \delta)|^2 (-\omega + \delta + \Delta) G_-^2. \quad (\text{E10b})$$

Comparing with Eq. (E5a), we see that the corrections have the same form, but with the frequencies interchanged. The reason that the picture is reversed is that $b^{(1)\dagger}$ rotates in sync with the upper drive and not with the lower one as $b^{(0)}$ does. In the case $\Delta = -\Omega, \omega = \Omega$, they are mirrored versions of Eq. (E5a)

$$\gamma' = \gamma + \frac{4}{\kappa} \left(\frac{G_-^2}{1 + 4\varepsilon^2/\kappa^2} - G_+^2 \right), \quad (\text{E11a})$$

$$\Omega' = \Omega + \frac{\varepsilon G_-^2}{\kappa^2/4 + \varepsilon^2}. \quad (\text{E11b})$$

We can neglect the second-order perturbation on the first order quantities $b^{(1)\dagger}, b^{(-1)}$, because they appear to third order on the level of spectrum calculations, such that

$$b^{(1)\dagger}(\omega) = -\chi_m^*(-\omega + \delta) \frac{2iG_+}{\sqrt{\kappa}} d_{\text{in}}. \quad (\text{E12})$$

In the main text we use the modified parameters $\tilde{\gamma}, \tilde{\Omega}$ in (24b). With this replacement, Eqs. (E6) and (E12) yield Eq. (29) It might seem surprising to use $\tilde{\gamma}, \tilde{\Omega}$ instead of γ', Ω' , but is allowed, as the corrections are third order. We mainly do that for convenience, because it makes the subsequent analysis more transparent. Comparing to the full solution and looking at Fig. 4, we see that our approximation is reasonable. In fact, we cannot use γ' , because it crosses zero for relatively small detunings $\varepsilon < \kappa$ when $\mathcal{C} > n_{\text{th}}$, which leads to a divergence.

In order to derive a master equation, we define $\tilde{b} \equiv e^{i\delta t/2} b$, and assume $\delta = 2\Omega$. Then $\beta \equiv (G_- \tilde{b} + G_+ \tilde{b}^\dagger)/\mathcal{G}$ obeys

$$\dot{\beta} = \left(-\frac{\gamma}{2} - \frac{2\mathcal{G}^2}{\kappa} \right) \beta + \sqrt{\gamma} \beta_{\text{in}} + \frac{2i\mathcal{G}}{\sqrt{\kappa}} \tilde{d}_{\text{in}}, \quad (\text{E13})$$

where $\tilde{d}_{\text{in}} \equiv e^{i\Omega t} d_{\text{in}}$. The associated quantum master equation is (NB in frame rotating with the mechanical frequency Ω)

$$\dot{\hat{\rho}} = \left(\gamma n_{\text{th}} \mathcal{D}[\tilde{b}^\dagger] + \gamma (n_{\text{th}} + 1) \mathcal{D}[\tilde{b}] + \frac{4\mathcal{G}^2}{\kappa} \mathcal{D}[\beta] \right) \hat{\rho}. \quad (\text{E14})$$

This agrees with Ref. [5]. The physics here is that the drives cool the Bogoliubov mode β close to its ground state, which is a squeezed state for the rotating quadrature $\tilde{b} + \tilde{b}^\dagger$ [5].

Appendix F: Analysis of instability within RWA

To study the instability we employ the Routh-Hurwitz criterion, according to which a system is unstable if the matrix M in $\dot{\mathbf{x}} = M\mathbf{x}$ has an eigenvalue with positive real part.

Let us call the matrix on the LHS of (D1) $K(\omega)$. In our case, $K(0) = -M$. Thus we can write $K(\omega) = -M - i\omega I_4$, where I_4 is the 4×4 identity matrix. The eigenvalues of $K(\omega)$ satisfy the secular equation

$$\det[-M - (i\omega + \lambda)I_4] = 0. \quad (\text{F1})$$

Thus, if λ is an eigenvalue of M , then $-\lambda + i\omega$ is an eigenvalue of $K(\omega)$. We conclude that if $\text{Re}[\lambda] = 0$, $K(\text{Im}[\lambda])$ is singular, and *vice versa*, which marks the onset of instability.

Assuming $\Delta = -\Omega$, it turns out that $\det[K(\Omega + \varepsilon/2)]$ is purely real and

$$\det[K(\Omega + \varepsilon/2)] = \sigma(\omega)\sigma(\omega - \varepsilon) - \varepsilon^2 G_+^2, \quad (\text{F2})$$

with $\sigma(\omega) = \mathcal{G}^2 + \chi_m^{-1}(\omega)\chi_c^{-1}(\omega)$ and $\delta = 2\Omega + \varepsilon$. Its imaginary part is zero at $\omega = \Omega + \varepsilon/2$, so we are left with

$$0 = \left(\mathcal{G}^2 + \frac{\gamma\kappa}{4} - \frac{\varepsilon^2}{4} \right)^2 + \frac{\varepsilon^2(\kappa + \gamma)^2}{16} - \varepsilon^2 G_+^2, \quad (\text{F3})$$

which gives

$$\varepsilon_{\pm}^2 = 4(G_-^2 + G_+^2) - \frac{\kappa^2 + \gamma^2}{2} \pm \sqrt{\left[\frac{\kappa^2 + \gamma^2}{2} - 4(G_-^2 + G_+^2) \right]^2 - (4\mathcal{G}^2 + \gamma\kappa)^2}. \quad (\text{F4})$$

ε_{\pm} is complex if the term under the root is negative, i.e., if

$$\mathcal{C} \leq \left(\frac{\kappa + \gamma}{2\sqrt{\kappa\gamma}} + \sqrt{1 + 2n_{\text{th}}} \right)^2. \quad (\text{F5})$$

In Eq. (F5) we have used the optimal driving strengths, see Eq. (41) or Ref. [5]. We conclude that there is an instability for $\varepsilon_- < |\varepsilon| < \varepsilon_+$. Note that the stability regions are symmetric in ε with stability at $\varepsilon = 0$. Because of condition (F5), we can only study large detuning for small cooperativities. As $\mathcal{C} \rightarrow \infty, \varepsilon_- \rightarrow \varepsilon_{\text{crit}} = \pm\sqrt{\kappa\gamma(1 + 2n_{\text{th}})}$, so there is a ‘‘stability corridor’’ in between $\pm\varepsilon_-$ even at largest cooperativities, which is shown in Fig. 6. Once we numerically include counterrotating terms, the stability corridor is lost. Note that we have assumed $\Delta = -\Omega$ and that if $G_+ > G_-$ the system may be unstable for all detunings δ .

Appendix G: The optical spectrum $S_{d^\dagger d}$

Following the same steps as in the main text, we can write the optical system operators in terms of the input operators

$$\begin{pmatrix} d^{(0)}(\omega) \\ d^{(1)\dagger}(\omega) \end{pmatrix} = \begin{pmatrix} \tilde{a}(\omega) & \tilde{c}(\omega) \\ \tilde{f}(\omega) & \tilde{g}(\omega) \end{pmatrix} \begin{pmatrix} d_{\text{in}}(\omega) \\ b_{\text{in}}(\omega) \end{pmatrix}. \quad (\text{G1})$$

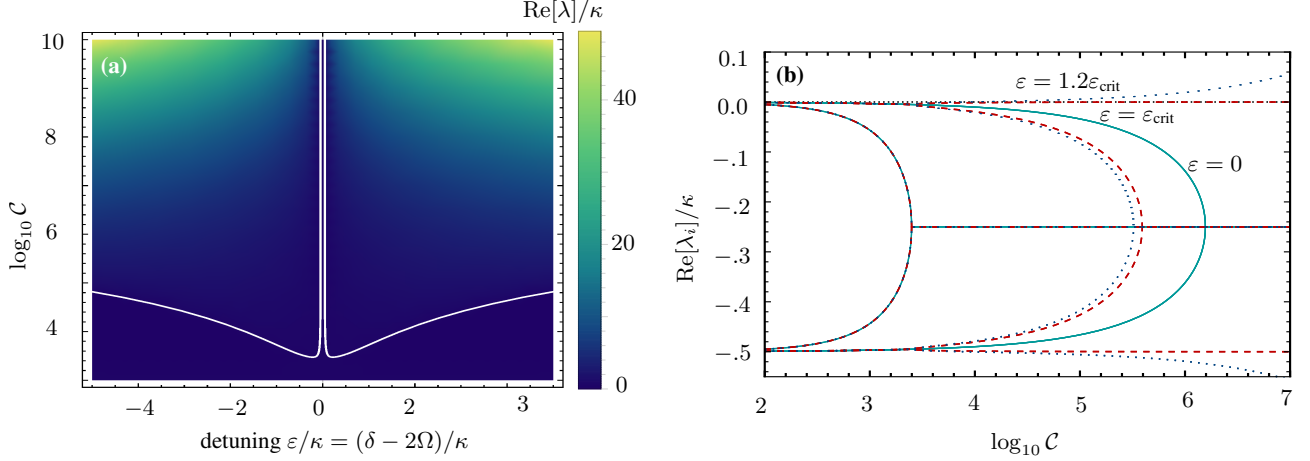


FIG. 6. **Analysis of instability within RWA.** Parameters are $\gamma/\kappa = 10^{-4}$, $n_{\text{th}} = 10$, $\mathcal{C} = 2 \times 10^3$, and $\Delta = -\Omega$. Ω/κ is irrelevant in RWA. **(a) Boundary of stability.** The white curve is the analytical result for the boundary of stability (F4). The color scale gives the real part of the eigenvalue with the largest real part λ of the matrix (D1). As $\mathcal{C} \rightarrow \infty$, a “stability corridor” remains, $\varepsilon_{\text{crit}} = \pm \sqrt{\kappa\gamma(1 + 2n_{\text{th}})}$. The corridor collapses without RWA. **(b) Eigenvalues as a function of cooperativity.** Real part of the eigenvalues of (D1) as a function of cooperativity \mathcal{C} for optimal driving Eq. (41), and detuning $\varepsilon = 0$, $\varepsilon_{\text{crit}}$, $1.2\varepsilon_{\text{crit}}$, in dark blue (solid), red (dashed) and turquoise (dotted). In the strictly stable regime all eigenvalues converge to have the same real part $(\kappa + \gamma)/4$ at large cooperativities \mathcal{C} . At the critical detuning two eigenvalues remain at $\gamma/2$ and two at $\kappa/2$ for all \mathcal{C} . Above the critical detuning, there exists a value of \mathcal{C} above which the system is unstable.

We obtain the functions in the matrix by a calculation analogous to the one in Appendix D. Because of the symmetry of the equations of motion in the RWA, this amounts to swapping $\gamma \leftrightarrow \kappa$, $\chi_c \leftrightarrow \chi_m$, $b_{\text{in}} \leftrightarrow d_{\text{in}}$. Thus,

$$\begin{aligned} \tilde{a}(\omega) &= \tilde{A}^{-1}(\omega)\sqrt{\kappa} \left[\chi_c^{-1*}(-\omega + \delta) + i\tilde{\Sigma}_{00}^*(-\omega + \delta) \right], \\ \tilde{c}(\omega) &= i\tilde{A}^{-1}(\omega)\sqrt{\gamma}\chi_m(\omega)G_- \\ &\quad \times \left[\chi_c^{-1*}(-\omega + \delta) + \mathcal{G}^2\chi_m^*(-\omega + \delta) \right], \\ \tilde{f}(\omega) &= -i\tilde{A}^{-1}(\omega)\sqrt{\kappa}\tilde{\Sigma}_{01}(\omega), \\ \tilde{g}(\omega) &= -i\tilde{A}^{-1}(\omega)\sqrt{\gamma}\chi_m(\omega)G_+ \\ &\quad \times \left[\chi_c^{-1}(\omega) + \mathcal{G}^2\chi_m^*(-\omega + \delta) \right], \end{aligned} \quad (\text{G2})$$

with

$$\begin{aligned} \tilde{A}(\omega) &= \left[\chi_c^{-1*}(-\omega + \delta) + i\tilde{\Sigma}_{00}^*(-\omega + \delta) \right] \\ &\quad \times \left[\chi_c^{-1}(\omega) - i\tilde{\Sigma}_{00}(\omega) \right] - \tilde{\Sigma}_{01}(\omega)\tilde{\Sigma}_{01}^*(-\omega + \delta), \end{aligned} \quad (\text{G3})$$

and

$$\begin{aligned} \tilde{\Sigma}_{00}(\omega) &= i \left[G_-^2\chi_m(\omega) - G_+^2\chi_m^*(-\omega + \delta) \right], \\ \tilde{\Sigma}_{01}(\omega) &= iG_-G_+ \left[\chi_m(\omega) - \chi_m^*(-\omega + \delta) \right]. \end{aligned} \quad (\text{G4})$$

The stationary part of the optical spectrum is

$$S_{d^\dagger d}^{(0)}(\omega) = |\tilde{c}(-\omega)|^2 n_{\text{th}} + |\tilde{f}(\omega + \delta)|^2 + |\tilde{g}(\omega + \delta)|^2 (n_{\text{th}} + 1). \quad (\text{G5})$$

Note that the same spectra can be obtained by employing the formulae in Sec. IV for the case $\delta = \delta_2$. As the mechanical spectrum one has to use the one derived in Appendix D, in

particular Eq. (47). Further note that the output spectrum is trivially related to $S_{d^\dagger d}$, since the input-output relation in our case is

$$d_{\text{out}} = d_{\text{in}} - \sqrt{\kappa}d, \quad (\text{G6})$$

such that

$$S_{d_{\text{out}}^\dagger d_{\text{out}}}^{(n)}(\omega) = \kappa S_{d^\dagger d}^{(n)}(\omega). \quad (\text{G7})$$

Appendix H: Readout spectra in second mode

In this section we provide more details on the calculation of the readout spectra. We split Eq. (42) into Fourier components

$$\begin{aligned} &\sum_{n,m} e^{in\delta t + im\delta_2 t} \left[(in\delta + im\delta_2) d_2^{(n,m)} + \dot{d}_2^{(n,m)} \right] \\ &= \sum_{n,m} e^{in\delta t + im\delta_2 t} \left[\left(i\Delta_2 - \frac{\kappa_2}{2} \right) d_2^{(n,m)} + \sqrt{\kappa_2} d_{2,\text{in}} \delta_{n,0} \delta_{m,0} \right. \\ &\quad \left. + i \left(G_{2+x}^{(n,m+1)} + G_{2-x}^{(n,m)} \right) \right]. \end{aligned} \quad (\text{H1})$$

If $\delta \neq \delta_2$ (and they do not have a common multiple), we have $b^{(n,m \neq 0)} = 0$. Thus, with $x^{(n,m)} \equiv b^{(n,m)} + b^{(n,m)\dagger}$,

$$d_2^{(n,0)} = \chi_2(\omega - n\delta) \left[\sqrt{\kappa_2} \delta_{n,0} d_{2,\text{in}} + iG_{2-x}^{(n,0)} \right] \quad (\text{H2a})$$

$$d_2^{(n,0)\dagger} = \chi_2^*(-\omega + n\delta) \left[\sqrt{\kappa_2} \delta_{n,0} d_{2,\text{in}}^\dagger - iG_{2-x}^{(n,0)} \right], \quad (\text{H2b})$$

$$d_2^{(n,-1)} = \chi_2(\omega - n\delta + \delta_2) iG_{2+x}^{(n,0)}, \quad (\text{H2c})$$

$$d_2^{(n,1)\dagger} = -\chi_2^*(-\omega + n\delta + \delta_2) iG_{2+x}^{(n,0)}. \quad (\text{H2d})$$

A substitution into Eq. (13) yields (46).

For the special choice $\delta_2 = \delta$,

$$d_2^{(n)}(\omega) = \chi_2(\omega - n\delta) \left[\sqrt{\kappa_2} \delta_{n,0} d_{2,\text{in}} + i \left(G_{2+x^{(n+1)}} + G_{2-x^{(n)}} \right) \right], \quad (\text{H3a})$$

$$d_2^{(n)\dagger}(\omega) = \chi_2^*(-\omega + n\delta) \left[\sqrt{\kappa_2} \delta_{n,0} d_{2,\text{in}}^\dagger - i \left(G_{2+x^{(n-1)}} + G_{2-x^{(n)}} \right) \right]. \quad (\text{H3b})$$

Again we substitute into Eq. (13) to get (48).

-
- [1] E. E. Wollman, C. U. Lei, A. J. Weinstein, J. Suh, A. Kronwald, F. Marquardt, A. A. Clerk, and K. C. Schwab, *Science* **349**, 952 (2015), [arXiv:1507.01662](#).
- [2] J.-M. Pirkkalainen, E. Damskagg, M. Brandt, F. Massel, and M. A. Sillanpää, *Physical Review Letters* **115**, 243601 (2015), [arXiv:1507.04209](#).
- [3] F. Lecocq, J. B. Clark, R. W. Simmonds, J. Aumentado, and J. D. Teufel, *Physical Review X* **5**, 041037 (2015), [arXiv:1509.01629v1](#).
- [4] A. Mari and J. Eisert, *Physical Review Letters* **103**, 213603 (2009), [arXiv:0911.0433](#).
- [5] A. Kronwald, F. Marquardt, and A. A. Clerk, *Physical Review A* **88**, 063833 (2013).
- [6] A. Papageorge, A. Majumdar, E. D. Kim, and J. Vučković, *New Journal of Physics* **14**, 013028 (2012).
- [7] M. Aspelmeyer, T. J. Kippenberg, and F. Marquardt, *Reviews of Modern Physics* **86**, 1391 (2014).
- [8] C. Gardiner and P. Zoller, *Quantum Noise: A Handbook of Markovian and Non-Markovian Quantum Stochastic Methods with Applications to Quantum Optics*, Springer Series in Synergetics (Springer, 2004).
- [9] A. A. Clerk, M. H. Devoret, S. M. Girvin, F. Marquardt, and R. J. Schoelkopf, *Reviews of Modern Physics* **82**, 1155 (2010).
- [10] V. I. Yudin, A. V. Taichenachev, and M. Y. Basalaev, *Physical Review A* **93**, 013820 (2016).
- [11] The Fourier components $\mathbf{x}^{(n)}(t)$ are not unique. Given a solution $\{\mathbf{x}^{(n)}\}$, transformations such as $\mathbf{x}^{(n)}(t) \rightarrow \mathbf{x}^{(n)}(t) + e^{ik\delta t} \mathbf{y}(t)$ and $\mathbf{x}^{(n+k)}(t) \rightarrow \mathbf{x}^{(n+k)}(t) - \mathbf{y}(t)$ lead to other solutions. However, these transformations leave the (physical) system operators $\mathbf{x}(t) = \sum_n e^{in\delta t} \mathbf{x}^{(n)}(t)$ invariant and we can show that the Fourier components of spectra are also unchanged. In the main text we choose to put the noise operators entirely in the zeroth component equation. The quantum Langevin equation is a first order ODE, which guarantees the uniqueness of its solution.
- [12] We will use the notions “measuring a rotating quadrature” and “measuring in a rotating frame” interchangeably. Of course, all measurements will always be performed in a lab frame, but it can be more intuitive to think about rotating frames instead.
- [13] A. A. Clerk, F. Marquardt, and K. Jacobs, *New Journal of Physics* **10**, 1 (2008), [arXiv:0802.1842](#).
- [14] The phase ϕ is primarily set by the relative phase of the lasers. In terms of their intensity beating, the squeezed quadrature can be found at or near the maximum intensity. They do not coincide if $\delta \neq 2\Omega$, in which case the squeezed quadrature lags slightly behind. The assumption that the coherent amplitudes \bar{a}_\pm are real leads to $\phi \approx \pi$ (equality if $\delta = 2\Omega$).
- [15] V. B. Braginsky, Y. I. Vorontsov, and K. S. Thorne, *Science* **209**, 547 (1980).
- [16] The lag of the squeezed quadrature behind the laser beating mentioned in Sec. III B is negligible for the physics that we would like to discuss. In addition, we will assume that the time scale on which the measurement is performed is large compared to any other time scale in the problem. If that were not the case, we could observe rotating spectrum components that decay as $\text{sinc}(\nu T)$ for their respective frequency ν and measurement time T .
- [17] G. Vasilakis, H. Shen, K. Jensen, M. Balabas, D. Salart, B. Chen, and E. S. Polzik, *Nature Physics* **11**, 389 (2015), [arXiv:1411.6289](#).
- [18] L. Ranzani and J. Aumentado, *New Journal of Physics* **17**, 23024 (2015), [arXiv:1406.4922v2](#).
- [19] J. Gea-Banacloche, N. Lu, L. M. Pedrotti, S. Prasad, M. O. Scully, and K. Wódkiewicz, *Physical Review A* **41**, 369 (1990).
- [20] R. Garcés and G. J. de Valcárcel, *Scientific Reports* **6**, 21964 (2016).